Available online at www.sciencedirect.com

jmr&t Journal of Materials Research and Technology

journal homepage: www.elsevier.com/locate/jmrt

Original Article

A study of an industrial counter pressure casting process for automotive parts

Jun Ou [a,*], *Chunying Wei* [a,b], *Savanna Logue* [a], *Steve Cockcroft* [a], *Daan Maijer* [a], *Yacong Zhang* [b], *Zhi Chen* [b], *Lateng A* [b]

[a] *The Department of Materials Engineering, The University of British Columbia, 6350 Stores Road, Vancouver, BC, V6T 1Z4, Canada*

[b] *CITIC Dicastal Co., Ltd, No 185, Long Hai Road, Economic and Technological Development Zone, Qinhuangdao City, Hebei Province, China*

ARTICLE INFO

Article history:
Received 23 June 2021
Accepted 24 November 2021
Available online 27 November 2021

Keywords:
CPC process
Plant trial
Data acquisition
Model development
ProCAST

ABSTRACT

Counter pressure casting (CPC) is emerging in the automotive manufacturing industry as an alternative to low-pressure die casting (LPDC) due to its reported superior capabilities in aluminum parts production. This study presents the first comprehensive investigation of how CPC's characteristic feature (applied chamber pressure) influences the fluid flow and heat transport occurring in the process and its effect on casting quality. A large amount of high-quality data was acquired from a commercial CPC process for the production of automotive suspension control arms with two process conditions (standard production and low back-pressure condition). Analysis of the data shows that there are no significant differences between the two process pressure conditions with respect to heat transfer during solidification, as-cast microstructure nor mechanical properties. Generally, in-die measured temperatures exhibited a difference within 10 °C for the two process conditions examined and the ultimate tensile strengths (UTSs) of the samples obtained from castings were within 7% for the two process conditions. Furthermore, there was no measurable difference observed in the Secondary Dendrite Arm Spacings (SDASs) obtained under the two process conditions. However, the implementation of chamber back pressure noticeably reduces the venting rate during the filling stage, leading to 12 s delay in the filling time relative to the low back-pressure condition. A computational modelling methodology, originally developed for LPDC, was applied to simulate the CPC process. The model required only an adjustment to pressure curve to account for the delay of filling owing to the reduced venting rate observed for the higher back-pressure condition. The predicted results were found to correlate well with the measured data, demonstrating that the modelling methodology is broadly applicable to permanent die casting processes.

* Corresponding author.
E-mail address: jun.ou@ubc.ca (J. Ou).

https://doi.org/10.1016/j.jmrt.2021.11.124

1. Introduction

Driven by the aggressive energy and emissions regulations and societal pressure, Original Equipment Manufacturers (OEMs) in the automotive industry have been increasing the use of aluminum [1,2]. The average mass of aluminum used per vehicle is predicted to increase by 55% by the year 2025 (250 kg) relative to 2011 (161 kg) [1]. This trend will continue as long as the cost-benefit of replacing low-strength ferrous castings with cast aluminum components is favourable. An example is the increased use of cast aluminum suspension parts such as knuckles and control arms [1].

For the production of cast aluminum parts, the two most widely used processes are low pressure die casting (LPDC) and high pressure die casting (HPDC) [3,4]. The LPDC process is primarily used for producing parts for load-bearing applications as it typically produces less defects, such as air entrapment and shrinkage porosity [5]. The HPDC process, on the other hand, can produce parts with complex geometries and smaller section thicknesses owing to its rapid filling procedure [6]. However, parts can suffer from air and oxide film entrainment. As part of ongoing improvement activities, the industry is working on advances in die design, innovative cooling technologies, and the development of novel processes [7,8]. For example, the counter-pressure casting (CPC) process, developed in the past decade, is a relatively new technology emerging in the casting industry as a suitable process for automotive part production [9–11]. It is claimed that the CPC process produces superior quality aluminum parts compared to the LPDC process as a result of the filling process occurring against a back pressure [9].

In recent years, computer-based simulation has augmented experience-based design to improve upon both die tooling and process parameter optimization [12,13]. The sophistication and accuracy of such models have progressed to the point where the prediction of shrinkage-related defect formation is quantitative from the standpoint of location, although prediction of the size distribution of pores remains challenging. Use of these models has led to improved cast quality and a reduction in time required to bring new parts into production [1,5,14–17]. One of the key requirements for developing these models and ensuring their veracity is the ongoing availability of high-quality, industrially derived data. Such data can be challenging to acquire owing to both technical and economical barriers.

This work presents an extensive characterization campaign to acquire process data undertaken on a commercial CPC process for the production of an aluminum alloy automotive control arm. The data acquired provides an opportunity to comprehensively and quantitatively assess the influence of applied die chamber pressure (back-pressure) on the filling and solidification behaviour. In addition, a modelling methodology, originally developed for an LPDC wheel production, has been applied to analyze the process under the conditions examined in the characterization campaign. This work will present thermal/pressure process data, an assessment of the accuracy and robustness of the modelling methodology and provide insights into the differences between CPC and LPDC processes. *Note: some confidential information related to the detailed design of the cooling elements has been removed for commercial reasons at the request of the industrial collaborator. The location of the cooling elements is provided together with the timing for activation of each element.*

2. Background and previous work

2.1. The CPC process

In comparison to the conventional LPDC process, the CPC process is a relatively new casting process for the manufacturing of automotive parts. The CPC process differs only in that the die system is placed inside a pressure chamber in which the pressure is elevated above atmospheric for die filling. Note: there is a variation of the LPDC process which also operates with the die in a pressure chamber; however, in this variant, the die cavity is at a reduced pressure during die filling.

Fig. 1(a) presents the basic structure of the CPC casting machine and die system. Fig. 1(b) shows the seven operational steps schematically. In Step (i), the die and pressure chamber are closed to begin the process. In Step (ii), the furnace and pressure chamber are simultaneously and equally pressurized. In Step (iii), the chamber pressure is held constant, while the furnace pressure is increased slowly. The resulting pressure difference ($\Delta P = P_{\text{furnace}} - P_{\text{chamber}}$) drives liquid metal up in the transfer tube and then into the die cavity. In Step (iv), after the die cavity is filled, the furnace pressure is quickly increased, followed by the release of chamber pressure. This achieves a high pressure difference (ΔP) so that solidification can occur under an intensified pressure. Step (v), the furnace pressure is released at the end of solidification and the remaining liquid in the sprue and transfer tube drops back to the furnace. Step (vi), the chamber and die are opened. Lastly, in Step (vii), the cast part is ejected from the die. The process is then repeated in a cyclic fashion. Prior to the start of casting campaign, the die system is preheated to a relatively high temperature (roughly 300–350 °C) using external heaters inserted into the die cavity. Once operational, the die temperature eventually reaches a cyclic steady state after completion of a few casting cycles.

In relation to the LPDC process, implementation of chamber pressure in the CPC process enables both filling and solidification to occur under a higher pressure. It has been claimed that the CPC process improves casting quality in several ways because of the increased pressure [9]. The first claim is that less oxide films are created and entrained because of a reduction in free surface turbulence. The second benefit is reported to be a more refined microstructure due to enhanced cooling rates caused by improved die/casting interfacial heat transfer. Lastly, a reduction in the number and/or size of shrinkage-based porosity is claimed due to solidification occurring at an increased pressure in comparison to the conventional LPDC process [18]. At present, however, there is no evidence obtained from a production casting that has been reviewed and published to support these assertions.

2.2. Previous computational modeling work

The incorporation of an analysis using a model is important in the present study in order to be able to critically interpret the

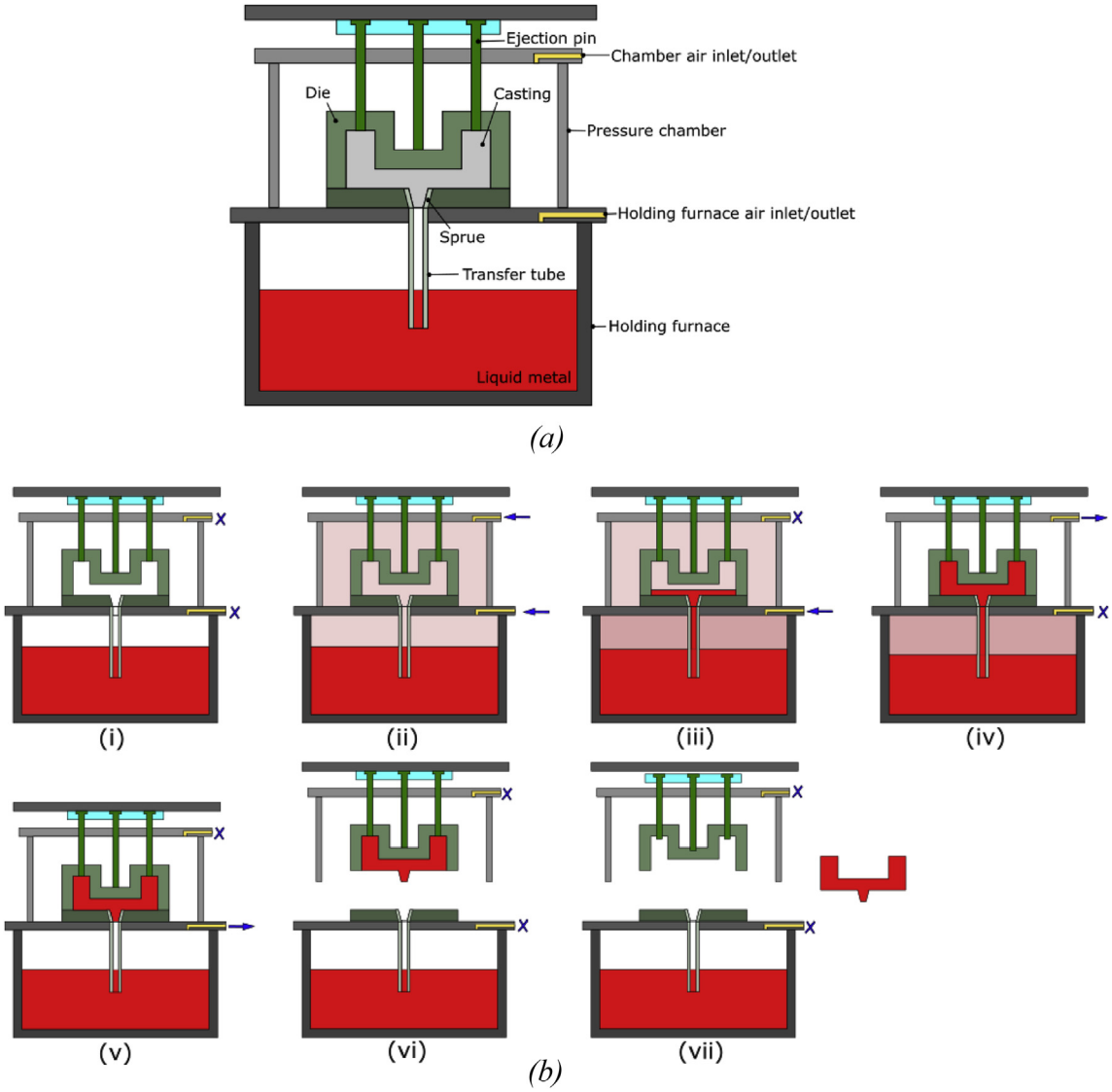

Fig. 1 – Schematic of the CPC machine and process procedure (a) Structure of the CPC machine (b) Major steps of the CPC process: (i) pressure chamber closed; (ii) furnace and pressure chamber are pressurized; (iii) furnace pressure is further increased slowly; (iv) chamber pressure is quickly released; (v) furnace pressure is released;(vi) chamber and die are opened; and (vii) the cast part is ejected.

process derived data. At present, there has been very little computational modelling work reported that is focused on the CPC process. One of the few studies is the model developed by Katzarov et al. [10], which is focused on predicting porosity formation in castings produced with various process parameters. A model was also developed by Georgiev et al. [19], which was applied to investigate both the CPC and LPDC processes. Fundamentally, these two processes can be described by the same modelling principles – i.e., a description of mould filling, heat transport during solidification and incorporation of the die temperature from the previous cycle as the initial condition for the subsequent cycle (to capture the cyclic nature of the process). As previously described, the major difference relates to the pressure regime during die filling and casting solidification. The pressure differential for die filling, $\Delta P = P_{furnace} - P_{chamber}$, where $P_{furnace}$ and $P_{chamber}$ are the pressure of the holding furnace and the chamber pressure, respectively. For LPDC, $P_{chamber}$ is the atmospheric pressure. For CPC, $P_{chamber}$ is elevated above atmospheric pressure for die filling. The pressure difference is similar – i.e. the driving force for die filling is similar - however, the filling occurs against a higher counter pressure in the CPC process.

3. In-plant process measurements

The in-plant process measurements were performed at a CITIC Dicastal manufacturing plant located in Qinhuangdao, Heibei, China. An operational, industrial-scale, CPC machine configured for the production of automotive suspension parts (control arms) was instrumented extensively and the data from these sensors was monitored with an in-house developed data acquisition (DAQ) system. Two types of data were collected: 1) PLC signals from the casting machine

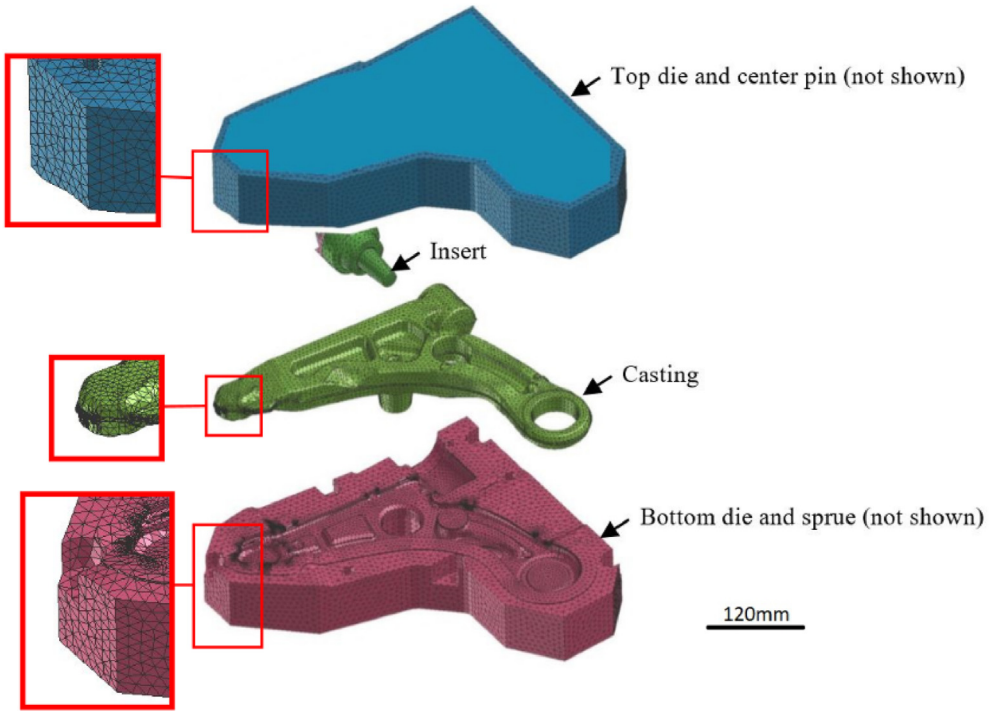

Fig. 2 – Geometry of the die sections and the cast component (control arm) and the mesh used for analysis.

identifying real-time operational stages - e.g., pressurization, filling, solidification, ejection - and 2) temperature data measured from thermocouples (TCs) installed at various locations within the die and the machine. The measurements were made over a number of cycles under cyclic steady-state casting conditions.

3.1. *Die and casting component*

Fig. 2 shows an exploded view of die sections and the cast component. Table 1 lists the materials used. The assembled die cavity is formed from three major parts: the top die (with a centre pin), the bottom die (with a sprue) and the insert. Note: the insert is used to create a hole on the side of the casting. The top die is cooled using seven water spot-cooling elements, while the bottom die does not have any forced cooling features. For confidentiality, the detailed structure of the water-spot-cooling elements are hidden from the figure, but their locations are schematically shown in Fig. 3.

3.2. *Process conditions*

Given that one of the major objectives of this work is to investigate the impact of chamber pressure, only the chamber pressure was varied while the remaining process parameters were held constant. Note: two pressure curves must be specified for the CPC process: $P_{furnace}(t)$ and $P_{chamber}(t)$. The first test condition was based on the standard CPC process parameters used for commercial production (labelled as CPC-SP). The second condition set the chamber pressure, $P_{chamber} = 0$ mbar-gauge, throughout the whole process, effectively mimicking the LPDC process (labelled as CPC-LP). Fig. 4(a) and (b) present the pressure curves specified for CPC-SP and CPC-LP process conditions, respectively. Fig. 4(c) shows the pressure differential (ΔP) curves for both conditions. The corresponding times, pressures and pressure differential (ΔP) associated with each of the Set-points (Sp's) for the two cases examined are listed in Table 3. The water-cooling schedules - e.g., on/off timings for each cooling element - for both process conditions were kept identical and are presented in Fig. 5. The locations of the cooling elements have been given previously in Fig. 3.

Referring to Fig. 4(c), it can be seen that the applied pressure difference is identical for both process conditions up to pressure intensification stage. This was meant to ensure the same driving force for fluid-flow during die filling for both processes. Filling of the die cavity is programmed to start at 18 s and finish before 32 s, as indicated in Fig. 4(c).

In the CPC-SP case, intensification occurs from 32 s to 37 s by a 140 mbar increment in the furnace pressure to yield a pressure differential of 300 mbar. This is followed by a second increment when the chamber pressure is exhausted to atmospheric pressure, yielding a further pressure differential increase to 2500 mbar, which also occurs over 5 s. In the CPC-LP case, pressure intensification also occurs from 32 s to 37 s by a 140 mbar increment in the furnace pressure to yield a pressure differential of 300 mbar and then by a second increment in furnace pressure of 500 mbar to yield a pressure

Table 1 – Parts and their materials.

Part	Material
Die Sections (top and bottom dies, and insert)	H13
Casting	A356

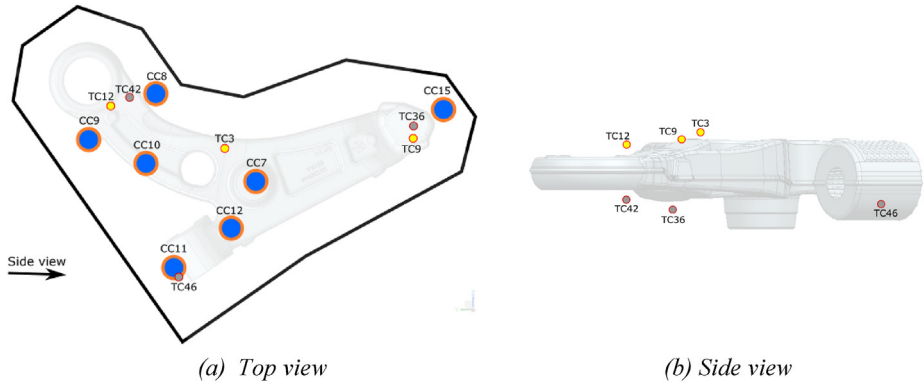

(a) Top view (b) Side view

Fig. 3 – Schematic showing locations of the cooling elements and TCs. Note: the distances between the TCs and die/casting interface are given in Table 2.

differential of 800 mbar. As there is a limit on casting machine's furnace pressure that can be applied when there is no chamber pressure, this limited the maximum pressure differential to 800 mbar. As a result, there is a difference in both the counter pressure during die filling and the pressure exerted on the component during solidification for the two process conditions examined.

Table 2 – Distances between the TCs and die/casting interface.

TC label	TC3	TC9	TC12	TC36	TC42	TC46
Distance [mm]	5.0	5.3	5.0	5.0	5.4	6.9

3.3. *Temperature data acquisition*

In total, 65 type-K TCs were installed in the die sections and on the machine at various locations - 31 in the top die, 13 in the bottom die, 5 in the environment surrounding the die, 9 in the cooling channels and 4 in the bottom plate that the die is mounted on. Additionally, 3 were cast into the component. *Note: the typical error of type-K TC in the temperature range of this work is less than 2.2 °C.* Data from the TCs was collected with a DAQ system at 4 Hz. The collected temperature data was used for four major purposes:

1. To aid in understanding the transport phenomena active during this casting process. For example, identification of

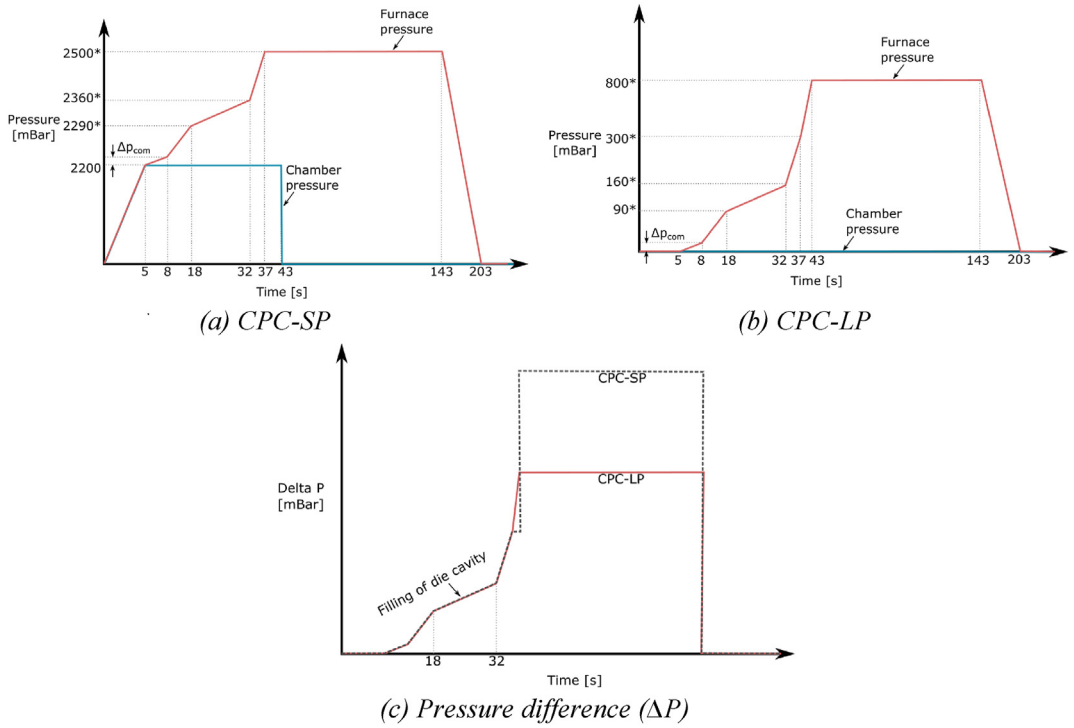

(a) CPC-SP (b) CPC-LP

(c) Pressure difference (ΔP)

Fig. 4 – Furnace pressure, chamber pressure and resulting pressure differential variation with time for the CPC-SP and CPC-LP process conditions.

Table 3 – Furnace and chamber pressure parameters and resulting pressure differentials used in the two process conditions.

Time (s)	Description	CPC-SP (mbar-gauge)	CPC-LP (mbar-gauge)	ΔP (CPC-SP/LP) (mbar)
5	Initial pressurization of the furnace and chamber	2200	0	0/0
8	Furnace pressure increase to compensation for the liquid level drop in the furnace due to consumption of metal – calculated.	Variable	Variable	0/0
18	Furnace pressure increase to force liquid up the transfer tube	2290[a]	90[a]	90/90
32	Furnace pressure increase to fill the die cavity	2360[a]	160[a]	160/160
37	First-stage furnace pressure intensification.	2500[a]	300[a]	300/300
43	Second-stage furnace pressure intensification	2500[a]	800[a]	2500/800
143	Pressure release is started	2500[a]	800[a]	2500/800
203	Pressure release is finished	0	0	0

[a] The calculated compensation pressure for liquid metal consumption (variable) is not included in these values.

heat transfer when boiling occurred within the water-cooling elements;
2. To identify and quantify boundary conditions. For example, the DAQ system measures the environmental temperature in the chamber, which was used in the model for describing the convective heat transfer from the die to the environment within the pressure chamber;
3. To validate the model;
4. To identify differences in the process resulting from the two sets of process conditions – i.e., with and without the chamber pressurized.

3.4. *Casting characterization*

For each process condition, a component was examined by X-Ray Computed Tomography (CT) to provided data on shrinkage-based porosity with features larger than ~ 0.5 mm. The castings selected for CT analysis were obtained from the process operating at a cyclic steady-state. This data will also be used to assess the model's capability to predict shrinkage-based porosity defects.

In addition to the CT analysis, two sections from each component were removed and examined using optical microscopy to characterize the secondary dendrite arm spacing (SDAS). One of these sections was cut from a region near the inlet, location B in Fig. 6(a), while the other was taken from a region far away from the inlet, location A in Fig. 6(a). In each sample, the SDAS was determined using the standard line-intercept approach [20]. This procedure was performed on four separate primary dendrites. These measurements were then divided by the number of secondary dendrites on each primary dendrite to get the SDAS, and then the mean of the four SDAS values was calculated.

Tensile samples were machined from each of the cast components - see sample locations TS1, TS2 and TS3 in Fig. 6(a). The dimensions of the tensile samples are shown in Fig. 6(b), which are in accordance with standard ASTM B 557M. The tests were performed on an Instron 3369 with the displacement control in accordance with ASTM E8. The test speed is 2 mm/min, and a clip-on strain gauge (Gauge Length 12.7 mm/0.5 inch) was installed to determine the strain.

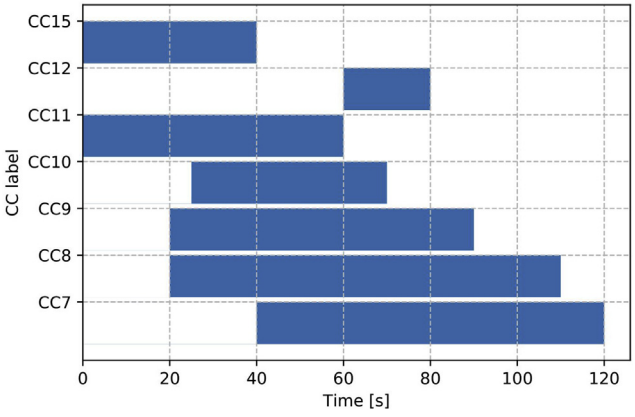

Fig. 5 – Cooling timings – refer to Fig. 3 (a) for the locations of cooling channels on the top die.

4. Computational model

The mathematical model of the CPC process was developed using ProCAST,[1] which uses the Finite Element Method (FEM). The software is capable of describing the transport phenomena occurring during the different stages of casting - i.e., die filling (momentum conservation/mass continuity), solidification (heat/conservation), die opening (heat/conservation), part ejection (heat/conservation), and die closing (heat/conservation). It is not capable of undertaking a two-phase analysis during die filling that could be used to account for the effect of counter pressure (2–3 bar) on venting and on free surface turbulence.

The CPC process model has been based on a previous model of an LPDC wheel casting process published by the authors (see reference [17]), which assumes perfect venting during the filling stage. For the most part, the parameters (material properties, boundary/interface conditions, and numerical parameters) used for the LPDC model have been applied without addition/modification for analysis of the CPC process. One addition/modification that was necessary was the formulation of a

[1] A trademark of ESI-Group.

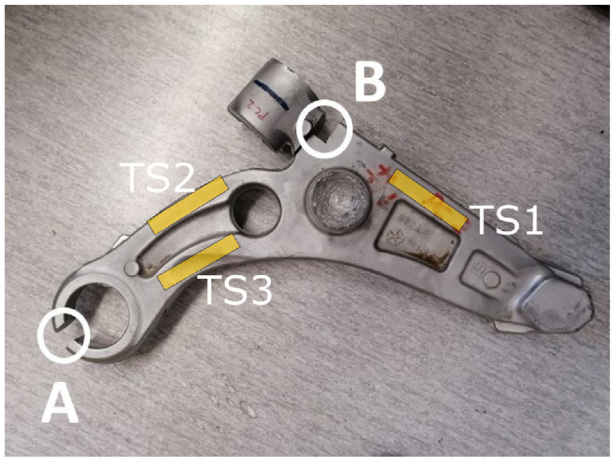

(a) Sampling locations

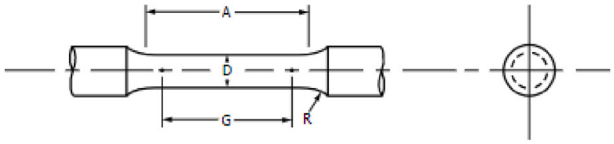

G (Gage Length) - 30.00±0.06 mm
D (Diameter) - 6.00±0.10 mm
R (Radius of Fillet)-6 mm
A (Length of Reduced Section) - 36mm

(b) Dimensions for tensile test samples

Fig. 6 – Samples removed from the control arm for microstructural analysis and tensile tests.

boundary condition to describe the heat transfer within the top die spot-cooling elements that use water (also sometimes referred to as cooling fingers). This addition/modification had to be made as the CPC process does not apply air-purging after turning off the water while the LPDC process does. Since many of the aspects of the two models are identical, only the differences will be discussed herein.

4.1. *Geometry and mesh*

The geometry (computational domain) and mesh used in the model have been presented earlier in Fig. 2. The mesh ranged in size from 2 to 10 mm and was configured to increase gradually moving away from areas of high heat transfer including the die/casting interface and the water cooling elements. The result was a mesh containing 73,996 surface cells and 448,137 body cells.

4.2. *Thermo-physical properties and initial conditions*

The thermo-physical properties for the die elements (H13) and casting (A356), are identical to those used in [17].

The CPC process is cyclic and the temperature distribution in the die at the end of each casting cycle serves as the temperature distribution in the dies at the beginning of the next cycle. If free of process parameter changes, the process will eventually reach a cyclic steady-state, where the temperature distribution at the start and end of each cycle is the same and invariant with time. Typically, there are a number of cycles required to reach cyclic steady-state at the beginning of a casting campaign and following a process upset. The model operates in the same manner with the temperature distribution in the dies at the end of a cycle input as the initial condition for the subsequent cycle. Cycle steady state is said to be achieved when the temperature change in the die, cycle-to-cycle, does not exceed a user input threshold of 5 °C.

4.3. *Boundary conditions*

There are two categories of boundary conditions: thermal and fluid flow.

4.3.1. *Thermal boundary conditions*

Water cooling – The water-cooling elements used to cool the die are carefully designed with respect to both location and on/off timing within a casting cycle. An example of a typical spot-cooling element is schematically shown in Fig. 7. In the model, the on/off timings correspond to those used in the plant trials (see Section 3.2). The heat transfer phenomena occurring within the water-cooling elements is typically highly non-linear with respect to die interface temperature both when the water is switched on and again when it is switched off. Initially, when water first enters the cooling element, the die is hot (300–500 °C) and boiling occurs until the die temperature is reduced. After this initial transient, heat is removed by forced convection. When water flow is turned off, heat continues to be extracted from the die at a high rate while residual water is present. Heat transfer during this transient typically shifts back to boiling until the water is "boiled off". Note: this may take some time if the water is replenished by the supply lines draining.

The methodology to describe the heat transfer occurring at the cooling locations is the same as that for the LPDC process. For the water-on stage, it is described by the following thermal boundary condition:

$$q_{cc} = h_{cc}(T_{surf} - T_{water}) \quad (1)$$

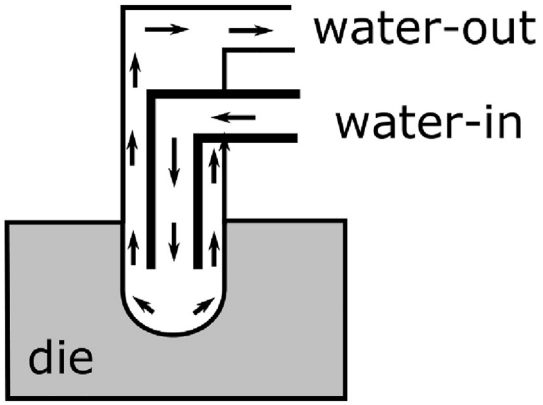

Fig. 7 – Schematic of spot or finger-type cooling element used in the CPC process.

where q_{cc} is the heat flux, h_{cc} is the heat transfer coefficient (HTC), and T_{surf} and T_{water} are the surface temperature of the die and water temperature, respectively. Readers are referred to [17] for details on the methodology used to calculate h_{cc} and set T_{water}.

When water flow is turned off, a constant heat flux (derived by trial-and-error) is applied to represent the heat removed by residual water as it boils off. It is acknowledged that this method is a simplified description that could be improved by using a more fundamental-based, temperature-dependent HTC for stagnant boiling. However, this requires the application of two temperature-dependent HTCs on one boundary that can only be implemented through the use of user-subroutines in ProCAST. User-subroutines were not supported in the version used for this study. The constant heat flux applied when the water is turned off is 3.0×10^5 W/m^2. Note that in the original LPDC model, this parameter was set to 1.5×10^5 W/m^2 to describe the heat transfer after flow was stopped. The rationale for increasing this parameter over what has previously been used is that after the cooling water is turned off in the CPC process, the cooling elements are not purged with air to quickly remove water as is the case for the channel-type cooling used in advanced LPDC wheel dies.

Environmental cooling - In the model, a HTC of 20 W/(m^{2}K) and an environment temperature of 85 °C (measured within the pressure chamber) are used to describe the convective heat transport from the external surfaces of the die. To capture radiative transport, an emissivity of 0.8 is used with the same environmental temperature. This boundary condition is applied to all surfaces that are exposed to the ambient environment in the pressure chamber. The temperature in the pressure chamber was found to be relatively stable and did not vary for the two process conditions examined in the study.

Temperature at the inlet - The thermal boundary condition at the fluid flow inlet is set to the temperature of the incoming metal - 700 °C. This temperature corresponds to the average temperature of liquid aluminum measured in the holding furnace.

Interface heat transfer - Heat transfer across the die/die and casting/die interfaces exhibits a variety of behaviour, including time, temperature and location dependence. For the die/die interfaces that continually maintain contact throughout the casting process, a constant interface HTC is applied. For the die/die interfaces that are periodic - i.e., that are present when the die section are closed and then are removed when the die sections are opened - a constant interface HTC is applied while there is contact, and when contact is broken, the environmental boundary condition previously described is applied.

For the casting/die interface, a relatively large initial HTC is applied to represent liquid metal in contact with the solid die during the filling stage. As the casting solidifies, the interface behaviour changes and becomes more complex. Depending on the location within the die, the interface can experience pressure, or conversely, gap formation, due to thermal contraction of the cast component and thermal expansion/contraction of the die as it is first heated and then cooled. In the current version of the model, two temperature-dependent interface HTCs have been adopted to describe the heat transfer associated with the aforementioned interface behaviour; one for the top die and the other for the bottom die. The correlations used in the model are presented in reference [17].

4.3.2. *Fluid flow boundary conditions*

Fluid flow during filling is driven by a pressure difference between the metal holding furnace and the pressure chamber. Currently, the model employs a pressure inlet boundary condition during the filling process. The computational domain does not include the transfer tube underneath the sprue, and therefore the pressure applied at the domain inlet has been modified to offset the pressure needed to fill the transfer tube – see Equation (2).

$$P_{inlet} = \Delta P - \rho_{A356} g h_{tube} \quad (2)$$

where P_{inlet} is the pressure applied at the domain inlet, ΔP is as previously defined, ρ_{A356} is the density of aluminum alloy A356, g is the acceleration due to gravity, and h_{tube} is the length of the transfer tube between the sprue and the liquid metal surface in the holding furnace. See also Table 3. The model assumes perfect venting during the filling stage and so there is no back pressure developed in the analysis. In addition, the model solves for fluid flow only during the filling stage of the process, which means that the effect of pressure intensification cannot be considered after the die cavity is fully filled and the inlet pressure is set to 0.

4.4. *Numerical convergence settings and parameters*

The default convergence criteria in ProCAST were assessed in a sensitivity analysis, and they were shown to be adequate. The time-steps were dynamically updated to meet the solution convergence criteria. Values of 0.001, 0.1, and 1 s were used for the initial time-step, the maximum time-step during filling, and the maximum time-step during solidification, respectively.

5. Results and discussion

5.1. *In-plant measurements*

5.1.1. *Temperature measurements*

Temperatures measured during the CPC-SP process at cyclic steady state are presented and discussed in this section. Namely, six TCs were selected to present the data: TC3, TC9, and TC12 in the top die; and TC36, TC42, and TC46 in the bottom die. The approximate locations of these TCs are given in Fig. 3 and their distances to the casting/die interface in Table 2. It can be seen that the selected TCs are sufficient to adequately provide an overall sense of the top die temperature and its evolution with time.

To begin, the extent to which cyclic steady sate was achieved is assessed by plotting the temperature measurements obtained from two thermocouples taken over three consecutive cycles (cycles 4–6) as a function of time within a casting cycle. Fig. 8(a) presents the data for TC3, located in the top die, and Fig.

8(b) for TC42, located in the bottom die. It can be seen that the thermal histories indicate excellent process stability.

Fig. 9(a) and (b) show the evolution in temperature during cycle 4 for the three representative TCs in the top die and three TCs in the bottom die, respectively. The temperature evolution at each TC location exhibits similar behaviour and is observed to have three stages: 1) a gradual decrease, following die-close; 2) a rapid increase in temperature as liquid metal enters the die and begins to solidify; and 3) a gradual decrease associated with casting solidification and the active cooling of the die.

The temperature evolution at individual TC locations is dependent on a combination of factors including: proximity to the metal inlet, proximity to the casting/die interface and proximity to any cooling elements (and their activation schedules). Comparing the temperatures at the TCs across the various locations, two observations are apparent:

1) TCs in close proximity to the inlet/sprue - e.g., TC3 - experience higher temperatures than those that are remote - e.g., TC9 and TC12. Temperatures at TC3 are in the range of 420–490 °C, TC9 is 340–450 °C, and TC12 is 260–370 °C. This drop in temperature is desired to promote the solidification regime starting at the furthest position from the sprue and generally moving toward the sprue, thereby providing a source of liquid to feed the Liquid/Solid density change.
2) There is more spatial variation in the temperature distribution in the top die compared to the bottom die. As can be seen in Fig. 3(b), thermocouple pairs TC12/TC42 and TC9/TC36 are located directly above one another (vertically aligned). TC9 and TC12, which are located in the top die, exhibit a much more significant temperature difference (70 °C) compared to that of TC36 and TC42 (30 °C). This phenomenon is observed because the top die is extensively cooled by seven water spot-cooling elements.

The temperature histories acquired from six example TCs, for the two process conditions (CPC-SP and CPC-LP), are compared in Fig. 10(a)–(f). The black and red solid lines are the measured temperatures from CPC-SP and CPC-LP conditions, respectively. As can be seen, the beginning of the second stage in temperature behaviour – i.e., when the heat from the liquid metal reaches the TC location and the temperature rises quickly - occurs ~12 s sooner in CPC-LP condition as compared to CPC-SP condition for the locations examined. This suggests that the die cavity is filled ~12 s earlier in CPC-LP process condition than in CPC-SP process condition. Referring to the pressure curves (see Fig. 4(c)), the two process conditions have identical pressure differential curves during the filling stage,

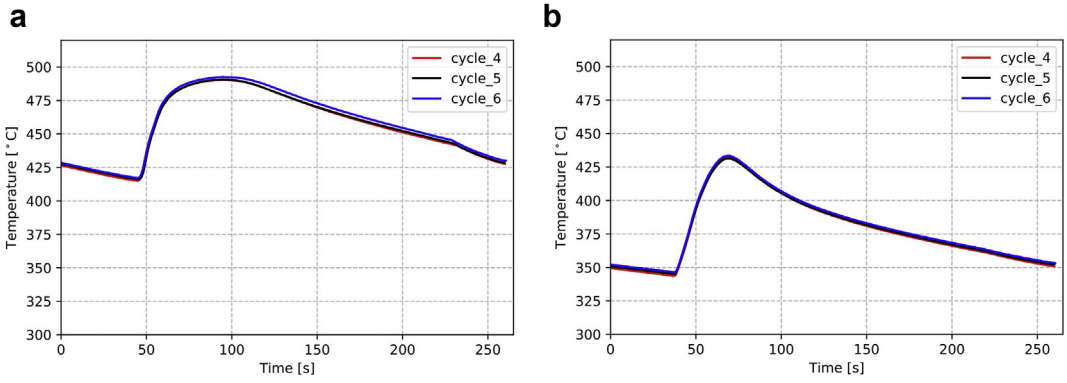

Fig. 8 – Temperatures measured from three sequential cycles.

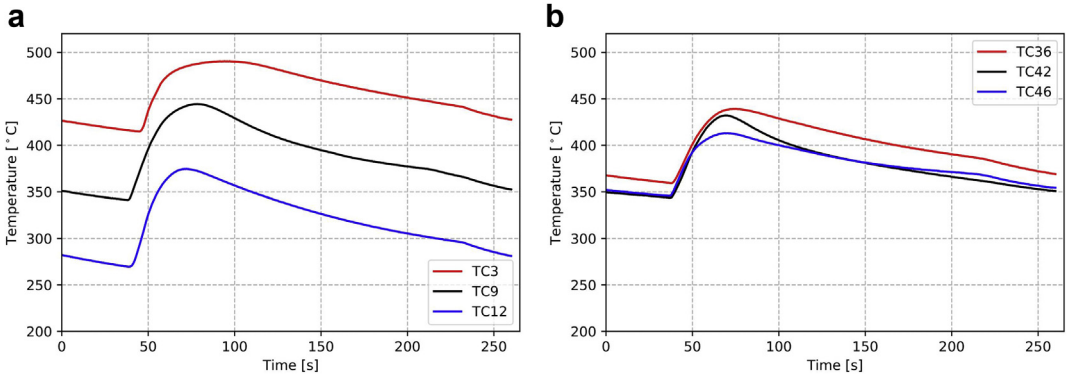

Fig. 9 – Temperatures measured by different TCs from a cyclic steady state cycle.

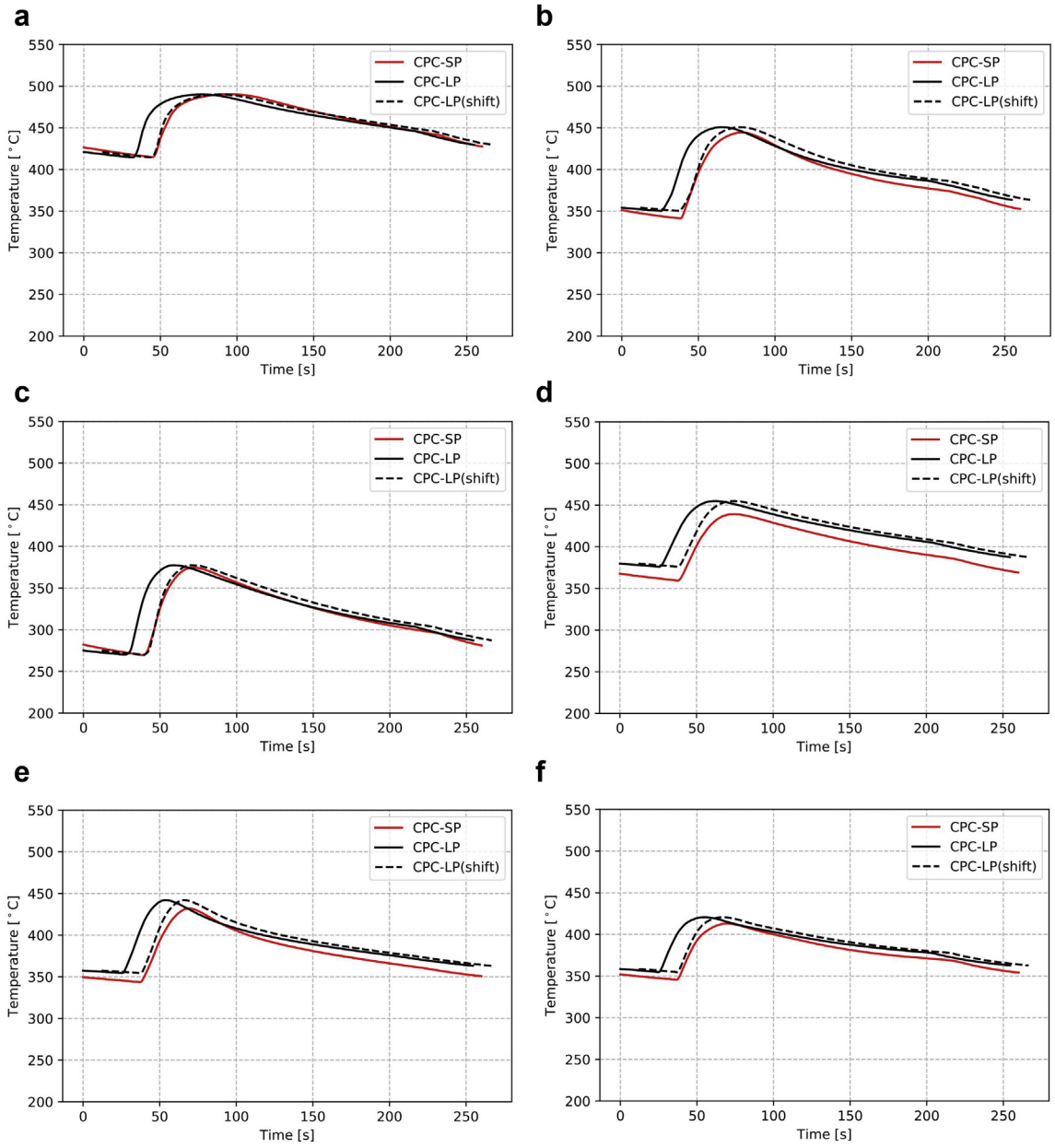

Fig. 10 – Comparison of temperatures measured from different process conditions.

and thus, the filling behaviour would be expected to be identical. One possible explanation is that filling is being affected by a difference in venting between the two cases. As previously defined, $\Delta P = P_{\text{furnace}} - P_{\text{chamber}}$ provides the driving force for die filling. This expression, however, is not strictly correct. The correct expression should be $\Delta P = P_{\text{furnace}} - P_{\text{die cavity}}$. During the filling process, if venting is not sufficient, a significant back pressure may form in the die cavity, which would reduce the driving force, slowing filling. As the die used in both process conditions (including the vents) are identical, it would appear therefore that venting is being inhibited in the CPC-SP case because of the elevated pressure in the chamber. When passing through the venting features of the die (which are thin gaps), the resistance (pressure drop across the vent) would be dependent on the air viscosity, which in turn would be affected by its pressure. To address this issue, a comparison of the post filling behaviour, a 12s shift to the CPC-LP data has been made and added to the graphs as the dashed black line.

Comparing the shifted CPC-LP data with the CPC-SP data, the temperature evolution at the locations examined in the die is very similar between the two process conditions. Most locations exhibit a difference in the range of 0–10 °C. The maximum difference observed is approximately 15 °C and occurred at TC36. This indicates that chamber pressure does not have a significant impact on the temperature field within the die. It has been claimed that die/casting interfacial heat transfer can be improved with the application of chamber pressure [9]. This claim is not supported by the temperature data measured in this work. Improved die/casting interfacial

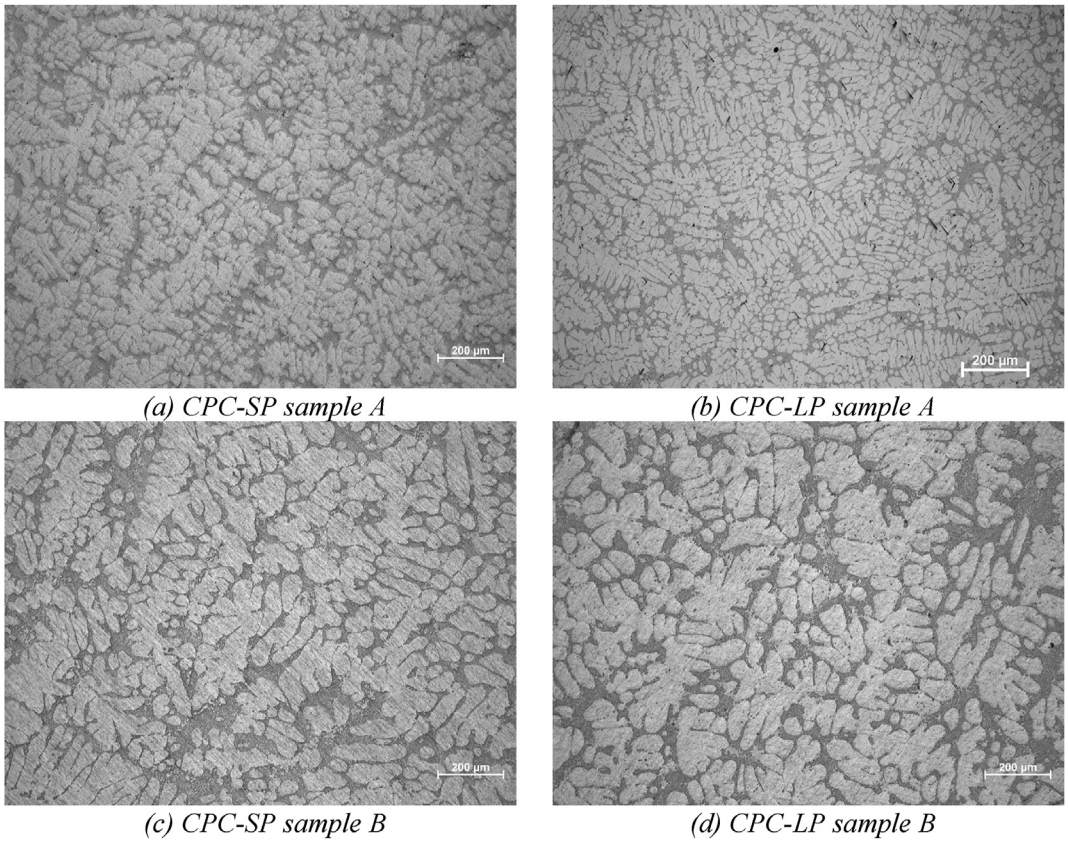

Fig. 11 – Optical microscopy observation of the samples.

heat transfer would elevate the die temperature. In contrast, it is observed that the die temperature in CPC-LP is slightly higher than that in CPC-SP.

5.2. *Microstructure and mechanical properties*

The microstructures obtained from location A for the two process conditions are shown in Fig. 11 (a) and (b) and for location B in Fig. 11 (c) and (d). These images were obtained optically and were prepared by polishing to 0.5 μm (no etch was used). The SDAS of each sample has been measured (average of 5 measurements) from these micrographs and reported in Fig. 12. The number appearing above each bar is the mean of the five measurements, and the standard deviation in the measurements have also been added and is indicated by the black line.

As can be seen, for both process conditions, the microstructure at location A is more refined than at B. This is because the cooling rate is higher at location A, which is located further from the sprue than location B. Comparing the two process conditions, the difference in the means at location A is ~25%, and at location B (~5%), with the CPC-LP process consistently yielding a smaller SDAS. However, it should be noted that the differences observed fall within the variability in the measurements and so no conclusion can be drawn.

The results of the tensile tests (as-cast samples) are shown in Fig. 13. Fig. 13(a) shows a typical tensile test curve and Fig. 13(b) shows a comparison between the UTS obtained from the three sample locations for the two process conditions. The three sample locations can be found by referring back to Fig. 6(a). Once again, there appears to be no significant difference in the results for the two process conditions examined.

5.3. *Modeling results*

The model of the CPC process has been used to predict the evolution in temperature within the die and casting for the process conditions examined in the plant trial. To begin, the variation in temperature predicted by the model in the die is compared with the measured temperatures to validate the model. The validated model was then used to examine the

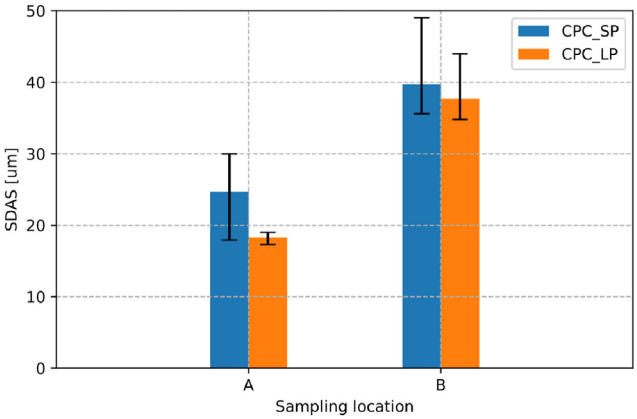

Fig. 12 – SDAS measurements.

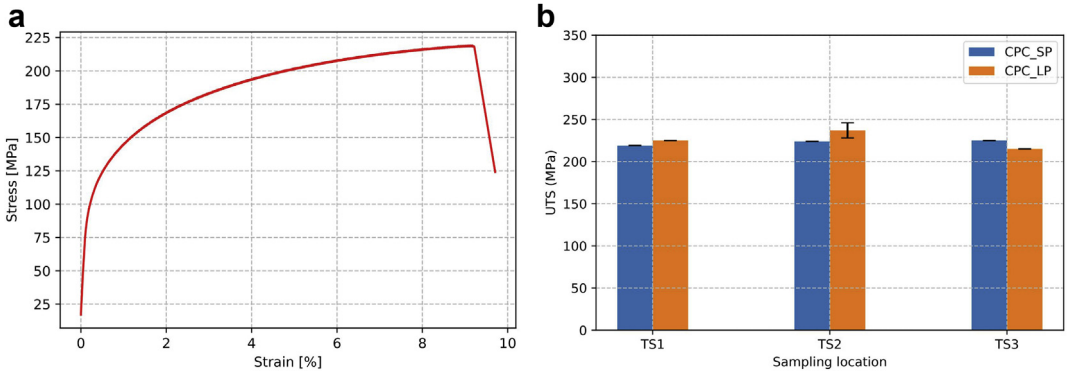

Fig. 13 – Tensile test results.

difference in filling to better understand the impact on the die/casting thermal field and the potential for defect formation.

5.3.1. *Die temperature*

The cyclic-steady state temperature history predicted by the model at the six representative TC locations is compared with the measured data in Fig. 14 (refer to Fig. 3 for TC locations). In general, the model predicted temperatures show reasonable agreement with experimental results. The level of agreement shown indicates that the model considers all of the key physical phenomena with respect to both heat transfer and fluid flow occurring in the CPC process. That said, it can be seen that at some locations - e.g., TC3 and TC9 - the fit is relatively poor, particularly when the die reaches its peak temperatures in the range of 60–120 s. One possible explanation for this discrepancy is that a simplified description of the casting/die interface behaviour is used in the model. Recent research has confirmed that the interface behaviour during the casting process is complex due to the potential to form both physical gaps and pressure after the die is filled and the casting begins to solidify [21]. A more quantitative description would require an understanding of the contraction of the casting and expansion/contraction behaviour of the die at various locations within the die, which is beyond the capabilities of the current model as it utilizes a positionally independent temperature-based correlation.

5.3.2. *Solidification sequence (shrinkage-based porosity)*

The solidification sequence predicted by the model has been used to assess likely locations of shrinkage-porosity formation. Ideally, directional solidification occurs such that solidification begins at the farthest point in the casting from the sprue before progressing gradually and sequentially toward the inlet/sprue. Failure to obtain directional solidification results in liquid encapsulation, which can cause shrinkage-based porosity.

To assess the potential for shrinkage, contours of the fraction solid in the casting in the range of 0–0.7 have been plotted as a function of cycle time in Fig. 15 for process condition CPC-SP. The sequence of images allows the progression of the solidification front within the casting to be observed. These results indicate that directional solidification is largely achieved. Only one small region of liquid encapsulation is observed in Fig. 15(b).

Porosity in the sample control arm obtained from process condition CPC-SP was examined by Computed Tomography (CT) imaging. The CT results shown in Fig. 16 confirm that there are no regions of large shrinkage porosity. However, two regions containing indications were identified – see Fig. 16(a). A close-up view of these locations, shown in Fig. 16(b), indicates the porosity to be small and distributed consistent with later stage (high f_s), solidification shrinkage.

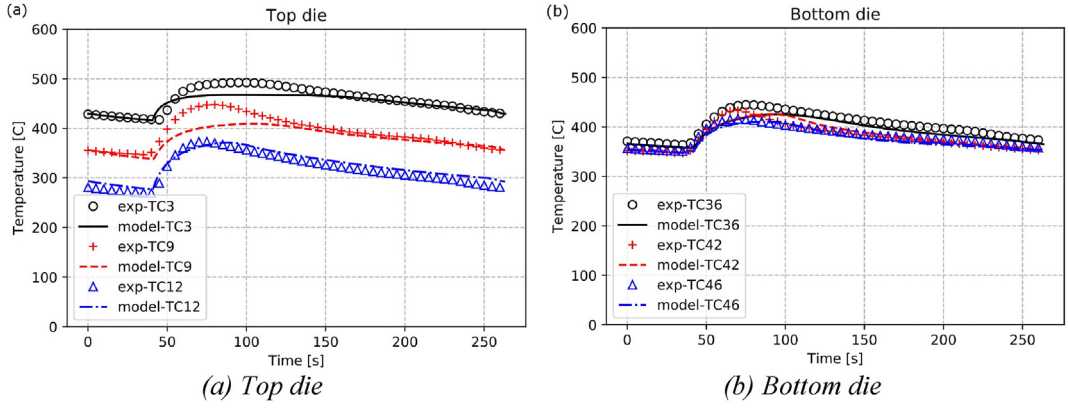

Fig. 14 – Temperature comparison between the model results and measured data.

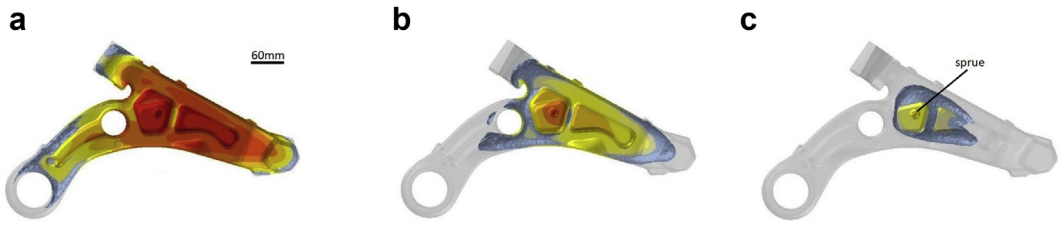

Fig. 15 – Solidification sequence - represented by contours of solid fraction limited to 0.7.

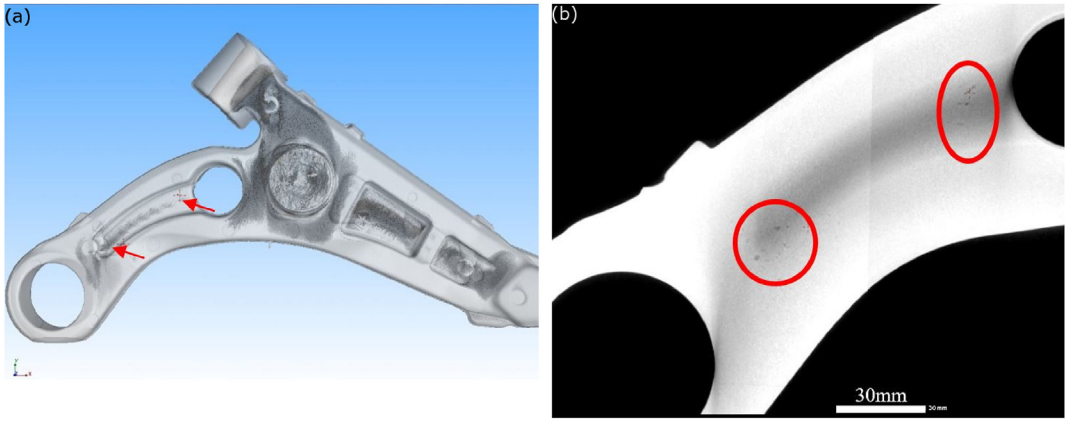

(a) macro view

(b) close up of region indicated to have some small distributed porosity

Fig. 16 – Location of porosity detected by CT scanning.

6. Summary and conclusion

For the first time, the effects of applied chamber pressure in the CPC process have been investigated and compared to the traditional LPDC process. Comparisons were made on a commercial CPC machine used to produce automotive control arms under two different process conditions. The first process condition was the standard operation and the second condition was using a lower (atmospheric) chamber pressure to emulate the conventional LPDC process. All the other process parameters were held constant.

Post casting analysis was done through a careful comparison of the in-die derived temperature data, a microstructural examination of metallographic samples taken from various locations, mechanical testing of samples taken from several locations in the casting and analysis of the results of a CT-Xray scan.

After analyzing the data from the two process conditions, it was found that an increased counter pressure during die filling significantly changed the filling behaviour, delaying filling by ~12s. This delay was speculated to be due to the larger resistance to venting associated with the increased viscosity of the air at the elevated pressure. Beyond this difference, the increased pressure differential during solidification does not significantly influence the evolution of the thermal field within the casting. No significant difference was observed in the TC-based data, in the microstructure-based data and in the tensile-based data.

A computational modelling methodology originally developed for LPDC process was applied to simulate the CPC process and further investigate the impact of counter pressure. The model was shown to be accurate, with little change to its formulation, other than to implement the boundary condition associated with splot-cooling elements (not present in the original LPDC model). It demonstrates that the developed modelling methodology is broadly applicable to permanent die casting processes for the production of various automotive parts.

Declaration of Competing Interest

The authors declare that they have no known competing financial interests or personal relationships that could have appeared to influence the work reported in this paper.

Acknowledgements

The authors acknowledge the financial and technical support of CITIC Dicastal Co., Ltd. for this work.

REFERENCES

[1] Martin Kahl XB. Special report: vehicle lightweighting. 2016.
[2] Isenstadt A, German J, Bubna P, Wiseman M, Venkatakrishnan U, Abbasov L, et al. Lightweighting technology development and trends in US passenger vehicles. Int. Counc. Clean Transp. Work. Pap. 2016;25.
[3] Bonollo F, Urban J, Bonatto B, Botter M. Gravity and low pressure die casting of aluminium alloys: a technical and economical benchmark. La Metall Ital 2005:23–32.
[4] Butler WA. *High pressure die casting*; encyclopedia of materials. Science and Technology; 2001.
[5] Zhang B, Maijer DM, Cockcroft SL. Development of a 3-D thermal model of the low-pressure die-cast (LPDC) process of A356 aluminum alloy wheels. Mater Sci Eng, A 2007;464:295–305. https://doi.org/10.1016/j.msea.2007.02.018.
[6] Collot J. Review OF new process technologies IN the aluminum die-casting industry. Mater Manuf Process 2001;16:595–617. https://doi.org/10.1081/AMP-100108624.
[7] Hu H, Chen F, Chen X, Chu YL, Cheng P. Effect of cooling water flow rates on local temperatures and heat transfer of casting dies. J Mater Process Technol 2004;148:57–67. https://doi.org/10.1016/j.jmatprotec.2004.01.040.
[8] Liu GW, Morsi YS, Clayton BR. Characterisation of the spray cooling heat transfer involved in a high pressure die casting process. Int J Therm Sci 2000;39:582–91. https://doi.org/10.1016/S1290-0729(00)00207-6.
[9] Vijayaram TR. CounterPressure casting techniquefor aluminium foundries. 2012.
[10] Katzarov IH, Arsov YB, Stoyanov P, Zeuner T, Buehrig-Polaczek A, Sahm PR. Porosity formation in axi-symmetric castings produced by counter-pressure casting method. Int J Heat Mass Tran 2001;44:111–9. https://doi.org/10.1016/S0017-9310(00)00085-5.
[11] Ou J, Wei C, Maijer D, Cockcroft S, Zhang Y, Chen Z, et al. Modelling of an industrial die casting process for the production of aluminum automotive parts. In: Proceedings of the IOP conference series: materials science and engineering, vol. 861. Institute of Physics Publishing; 2020. p. 12030.
[12] Zhu J, Cockcroft S, Maijer D. Modeling of microporosity formation in A356 aluminum alloy casting. Metall Mater Trans A 2006;37:1075–85. https://doi.org/10.1007/s11661-006-1027-5.
[13] Reilly C, Duan J, Yao L, Maijer DM, Cockcroft SL. Process modeling of low-pressure die casting of aluminum alloy automotive wheels. JOM 2013;65:1111–21. https://doi.org/10.1007/s11837-013-0677-1.
[14] Duan J, Maijer D, Cockcroft S, Reilly C. Development of a 3D filling model of low-pressure die-cast aluminum alloy wheels. Metall Mater Trans A 2013;44:5304–15. https://doi.org/10.1007/s11661-013-1654-6.
[15] Yao L, Cockcroft S, Zhu J, Reilly C. Modeling of microporosity size distribution in aluminum alloy A356. Metall Mater Trans A 2011;42:4137–48. https://doi.org/10.1007/s11661-011-0811-z.
[16] Ou J, Wei C, Cockcroft S, Maijer D, Zhu L, A L, et al. Advanced process simulation of low pressure die cast A356 aluminum automotive wheels — Part I, process characterization. Metals (Basel). 2020;10:563. https://doi.org/10.3390/met10050563.
[17] Ou J, Wei C, Cockcroft S, Maijer D, Zhu L, A L, et al. Advanced process simulation of low pressure die cast A356 aluminum automotive wheels—Part II modeling methodology and validation. Metals (Basel). 2020;10:1418. https://doi.org/10.3390/met10111418.
[18] Jahangiri A, Marashi SPH, Mohammadaliha M, Ashofte V. The effect of pressure and pouring temperature on the porosity, microstructure, hardness and yield stress of AA2024 aluminum alloy during the squeeze casting process. J Mater Process Technol 2017;245:1–6. https://doi.org/10.1016/j.jmatprotec.2017.02.005.
[19] Georgiev GE, Stanev L, Georgiev M, Maneva A, Stanev S. Optimization OF the process OF casting formation BY CPC method using computer simulation. 2017.
[20] Vandersluis E, Ravindran C. Comparison of measurement methods for secondary dendrite arm spacing. Metallogr. Microstruct. Anal. 2017;6:89–94. https://doi.org/10.1007/s13632-016-0331-8.
[21] Wei C, Ou J, Fan P, Mehr F, Maijer D, Cockcroft S, et al. Toward the development of a thermal-stress model of an industrial counter pressure casting process. In: Proceedings of the IOP conference series: materials science and engineering, vol. 861. Institute of Physics Publishing; 2020. p. 12062.